*Progress In Electromagnetics Research, Vol. 165, 13–33, 2019*

# Performance Improvement and Antenna Design of Left-Handed Material Units Based on Topological Deformations

**Baiqiang You[1], Mengyin Dong[1], Jianhua Zhou[1, *], and Haike Xu[2]**

**Abstract**—In this paper, by applying topological theory, we evaluate some left-handed unit structures. Based on the classification of topological deformation, the laws and characteristics of potential electromagnetic parameters are captured. The original left-handed material unit is realized by using a circular C-shaped coupling ring, whose whole size is $10\times10\times0.5$ mm$^3$. Through three kinds of topological deformations, to explore the influence of topology on antenna performance, the electromagnetic parameters and left-handed characteristics of the original and modified units are compared and analyzed. For the designed handshake-shaped unit structure, simulation analysis predicts that dual-frequency, or even multi-band left-handed characteristics, can be achieved. To expand the structural performance of the handshake-shaped unit, an annular line for coupling enhancement is added inside the U-shaped structure to form an integrally coupled annular unit structure. Simulation results show that, with amplitudes of reflection coefficients of $-27.1$ dB and $-14.5$ dB, the resonance points of the improved unit structure are 3.57 GHz and 5.64 GHz, respectively. Loading the unit structure with a dual-band left-handed characteristic, a UWB antenna is designed and analyzed in detail. Through simulation, antenna performance is most affected by interference within the range of $2.5 \sim 5.0$ GHz, which coincides with the double negative frequency band of the loaded left-handed structural unit. The notch frequency band of the designed UWB antenna, which is much wider than traditional notch antennas, is $3.62 \sim 4.54$ GHz, with a notch bandwidth of 920 MHz.

## 1. INTRODUCTION

The transmission mode, $(k, \overrightarrow{\mathbf{E}} \times \overrightarrow{\mathbf{H}})$, for a conventional uniform transmission line, satisfies the right-handed relationship shown in Fig. 1(a). The direction of $\overrightarrow{\mathbf{E}} \times \overrightarrow{\mathbf{H}}$ conforms to the right-handed rule for $k$, referred to as a right-handed transmission line [1], whose equivalent circuit can be regarded as the combination of a series inductance and a shunt capacitance (See Fig. 1(b)). According to transmission line theory, a left-handed medium is equivalent to the combination of a series capacitance and a shunt inductance [2] (See Fig. 1(c)). The biggest difference between Left-Handed Materials (LHMs) and Right-Handed Materials (RHMs) is the series and parallel connection relationships between the capacitors and inductors.

Because of the unique Double Negative Characteristics (DNCs) [3–5], the loading LHMs can achieve miniaturization, directionality, and high gain for an improved antenna. The realization of LHMs mainly includes two major types: resonance and transmission line types [6–12]. As to a classic structure, the resonance type uses a metal strip combined with a resonant ring, whereas the transmission line type uses a cross-connected series capacitor branch and a parallel stub. For LHMs with two or more left-handed passbands, based on resonant structures, the sizes or patterns are changed, so there are different resonant circuits in the equivalent circuits of the unit structures. A small antenna using periodic array of E-shaped unit cells can achieve good radiation properties and obvious bandwidth enhancement [13].

*Received 16 January 2019, Accepted 31 May 2019, Scheduled 10 June 2019*
* Corresponding author: Jianhua Zhou (eezhoujh@xmu.edu.cn).
[1] Department of Electronic Engineering, Xiamen University, Xiamen, Fujian, China. [2] Xinghai Communication Science and Technology Co., Ltd., Fuzhou 350008, China.

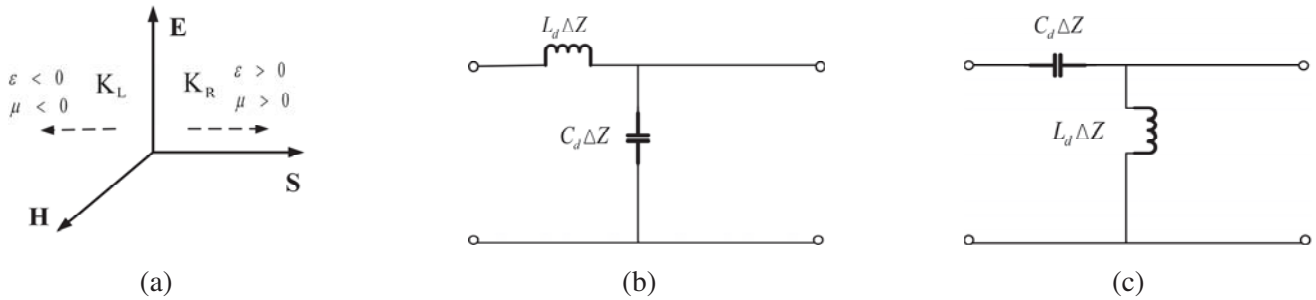


**Figure 1.** Characteristics of LHM and RHM. (a) Transmission mode of a RHM and LHM, (b) equivalent circuit of a RHM, (c) equivalent circuit of a LHM.

To enhance the gain and radiation efficiency of the antenna, Alibakhshikenari et al. [14] proposed an LHM Traveling-Wave Antenna (TWA) based on a metamaterial transmission-line structure. The LHMs with a multi-pass belt, including triangular opening rings of different sizes, are widely used to construct a double-pass LHM [15], an oblique triangular opening double-sided LHM with DNCs, etc. The three-way belt LHM is realized by forming a different magnetic resonant loop based on a tree-shaped fractal structure [16].

Topology means that the properties of a graph remain unchanged after a topological transformation [17, 18]. The intrinsic and qualitative features of geometric shapes, unaffected by changes in sizes and shapes, are studied mainly in topology. To better distinguish the changes in the shape of a graph or structure, it can be divided into three types of deformation according to the intensity of the topological change: differential homeomorphic, homeomorphic, and non-homeomorphic.

**Differential homeomorphic deformation.** In the process of differential homeomorphic deformation, only minor shape changes occur, in which there is no interference with the normal flow direction. The current and electric field distributions have high inheritance with the original structure, and the electromagnetic characteristics are continuously gradual.

**Homeomorphic deformation.** Homeomorphic deformation refers to a relatively obvious change in the structure, but the overall performance and structure are unchanged. Thus, the current and electric field distributions are less affected, and the electromagnetic characteristics may exhibit parasitic frequency characteristics.

**Non-homeomorphic deformation.** Non-homeomorphic deformation refers to the existence of structural fracture or convergence; increases and decreases in the number of fractures or convergences affect the overall current flow and electric field distribution. Also, there may be multiple variations in electromagnetic characteristics.

According to transmission line theory, changing the length of a transmission line is a continuously gradual change in a reactance. From the perspective of topology, a change in the length of a transmission line is also a kind of continuous topological extension, which has the same point as a continuous change in electromagnetic properties. Nevertheless, a cut in a continuous transmission line is another kind of topological change. Therefore, it is expected that a change in unit topology has some correlation with a change in electromagnetic parameters, leading to both continuity and discontinuity properties. For a transmission line structure, if the intermediate line breaks into two lines, the topology of the pattern will change, and the corresponding electromagnetic parameters will also change. From the perspective of topology deformation, there is an essential difference between an LHM and an RHM. The mutual conversion between parallel capacitance and inductance cannot be realized by the change in length of a single structure. Such changes are made only by non-homeomorphic deformation. The two consecutive extended structures change from the original simple series inductance to a series with a capacitance in the middle. Series capacitance, or series inductance, is the essential difference between the equivalent circuits of an LHM and an RHM.

In the early research of metamaterials, Split-Ring Resonators (SRRs) were proposed [19]. According to topology, there is a certain relationship between SRRs and traditional microstrip dipole antennas. Compared with a dipole antenna, an SRR is relevant to the intermediate fractured part of the pattern structure. The two sides change from the original linear shape to a curved one, thereby coupling the two

curved arms to generate a series capacitor. For electromagnetic characteristics changing from traditional RHM to LHM, we refer to non-homeomorphic topology deformation and discontinuity in the properties of the pattern structure. Haghighi et al. [20] proposed a three-band Leaky-Wave Antenna (LWA) based on a Composite Right/Left-Handed (CRLH) structure composed of two adjacent interdigital slots. From a single interdigitated structure to two interdigitated structures, combined with topology analysis, the inductive characteristics are introduced between the interdigitated fingers with discontinuous changes in the structure. On one hand, through non-homeomorphic changes, including two structures distributed left and right with series induction capacitors loaded, electromagnetic characteristics are discontinuously changed, resulting in left-handed characteristics. On the other hand, the interdigital structure itself provides series inductance, and the right-handed characteristic remains in some frequency bands. Because of the mutual coupling between unit structures, additional frequency points may be excited, and multiple bands may appear. A novel antenna, with a triple resonant frequency, is designed for each unit of the fork-shaped radiating element, and three radiating element array antennas are formed [21]. Because of the interaction between the units, the generated array antenna has a hexa-band.

The essence of traditional LHMs is the use of metal wires, or metal sheets, to limit the flow of current electrons. When the magnetic field generated by the current is strong enough and interferes with the original magnetic field, it is possible to produce a Negative Magnetic Permeability (NMP). Therefore, it is still insufficient to analyze the LHMs and capture structural features based on topological theory. Here, the combination of the structure diagram and electric field pattern is expected to achieve higher guidance. At present, there are few studies on antenna topological deformations in relative fields. For the first time, topological deformations are related to the modifications in the antenna characteristics. By performing three topological changes on the established base model, the characteristics of the antenna, with electromagnetic parameters modified by each topological deformation, are analyzed. The electromagnetic parameter variations are closely related to the topology, where the topology concept is used to explore the correlation between shape structure and classical parameters. The ways to analyze are advanced and feasible and, in some respects, may be superior to traditional field and numerical solutions.

## 2. TOPOLOGICAL DEFORMATION

### 2.1. Unit Design

Based on the design concept of an SRR ring, negative permeability is realized by the combination of a circular C-shaped ring and an interaction ring. For the unit structure shown in Fig. 2, the C-shaped ring, an open loop structure, is designed to ensure the inductance of the connected external metal strip and the capacitance of the external ring. The internal metal strip structure with a circular patch ensures parallel inductance. The size of the entire square unit structure is set as $L \times L$, along with the following: the distance between the upper and lower units as $h_1$; the thickness of the dielectric plate as

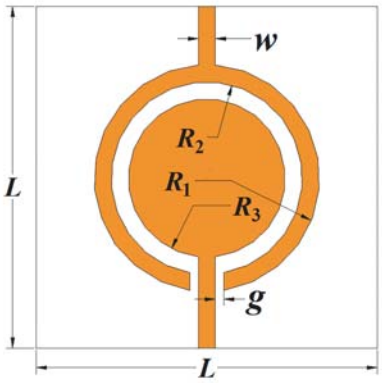


**Figure 2.** Schema of the designed unit.

$h$; the outer and inner radii of the metal C-shaped ring as $R_1$ and $R_2$, respectively; the radius of the circular patch as $R_3$; the width of the metal strip as $w$; and the gap between the two patches at the opening as $g$. The dielectric substrate, on which there is a 0.02 mm thick copper layer, is a commonly used FR4 dielectric material with a relative dielectric constant of 4.4 and loss tangent angle of 0.02. In general, the left-handed structural unit is not uniform, but considered as a homogeneous medium when it is small enough to reach between one-twentieth and one-quarter of the wavelength [22]. From the perspective of topology, the C-shaped unit is regarded as a circular structure with bilateral symmetry.

### 2.2. Theory Analysis

For an electromagnetic wave passing through the circular-C-shaped unit in the $x$-direction, a capacitance is formed between the C-shaped ring and the circular patch. The left and right sides of the C-shaped ring appear to be two parallel plates perpendicular to the direction of propagation; thus, the capacitance is regarded as a series capacitor. Current flows in the $z$-direction on the outer C-shaped ring and inner circular patch, which are considered shunt inductors. From the equivalent circuit diagram for both sides of the C-shaped ring, it is seen (Fig. 3) that the equivalent circuit of the C-shaped ring coupling is just opposite to that of the conventional structure, with the connection of the capacitors in series and the inductors in parallel. For unit capacitance, $C_d$, the following equation is used:

$$C_d = \frac{M\varepsilon_r s}{4\pi k(R_2 - R_3)} \tag{1}$$

where $\varepsilon_r$ is the relative dielectric constant; $k$ is the wave number; $M$ is an empirical factor with a value between 0.2 and 0.3; $s$ is the relative effective area of the inner and outer rings.

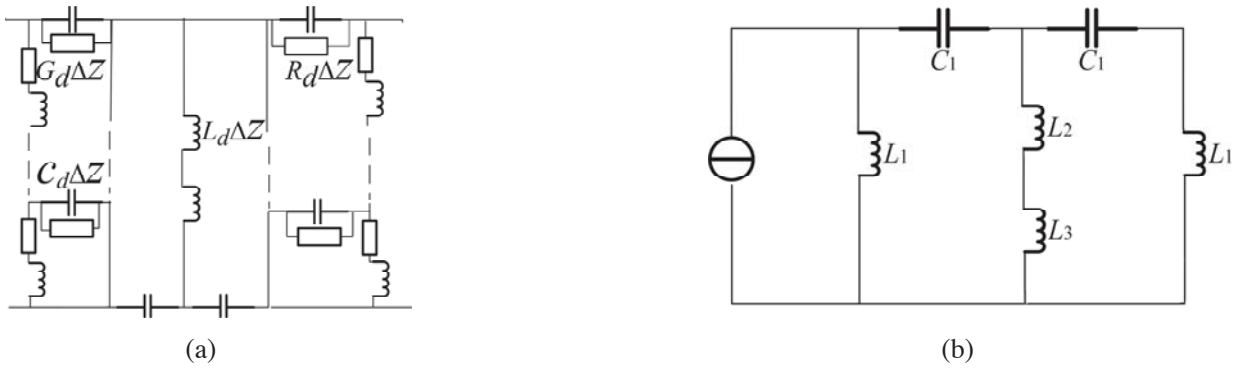


**Figure 3.** Equivalent circuit diagram of the overall unit structure. (a) Detailed, (b) simplified.

The equivalent circuit diagram for the overall structure of the designed unit is represented in Fig. 4. $C_1$ is the total capacitance of the metal C-shaped ring and two sides of the circular patch, including the capacitance, $C_d$, in the form of a transmission line and the gap capacitance, $C_g$, formed between the end of the C-shaped ring and the metal stick.

$$C_1 = \frac{C_d \cdot \pi(R_2 + R_3)}{2} + C_g \tag{2}$$

where

$$C_g = \frac{\varepsilon_0}{2\pi} \ln \frac{2(R_1 - R_2)}{R_2 - R_3} \tag{3}$$

The total capacitance of the loop is $C_{\text{total}} = 2C_1$; therefore, the capacitance of the resonant circuit is modified by adjusting the inner radius of the C-shaped ring and the outer radius of the circular patch. $L_1$ is the total inductance for both sides of the C-shaped ring. $L_2$ and $L_3$ are the inductances of the circular patch and the straight metal wire, respectively. For the total inductance, the relationship between the magnetic flux and the cell structure current is expressed as follows:

$$L_{\text{total}} = \frac{\Phi}{I} \approx \frac{\mu_0 \pi R_1^2}{h_1} \tag{4}$$

where $h_1$ is the spacing of the unit structure along the direction of the magnetic field $H$, and $\mu_0$ is the permeability, with a value of $4\pi \times 10^{-7}$ (H/m), in a vacuum.

With the equivalent total capacitances and inductances of the cell structure, the left hand transmission line theory can be used for analysis. For the medium as uniform, the unit length capacitance and inductance are $L \cdot C_{\text{total}}$ and $L \cdot L_{\text{total}}$, respectively, where $L$ is the length of the unit structure. According to the following voltage law,

$$\frac{V(z+\Delta z)-V(z)}{\Delta z} = -I(z)\left(\frac{1}{j\omega L \cdot C_{\text{total}}} + j\omega L_{\text{total}}\right) \tag{5}$$

where

$$Z = \frac{1}{j\omega L \cdot C_{\text{total}}} + j\omega L_{\text{total}} \tag{6}$$

we find that

$$\frac{\mathrm{d}V(z)}{\mathrm{d}z} = \frac{V(z+\Delta z)-V(z)}{\Delta z} = -Z \cdot I(z) \tag{7}$$

$$\frac{\mathrm{d}I(z)}{\mathrm{d}z} = -Y \cdot V(z) \tag{8}$$

and

$$Y = j\left(\omega C_R - \frac{1}{j\omega L \cdot L_{\text{total}}}\right) \tag{9}$$

The propagation constant is obtained from simultaneous Eq. (7) and Eq. (9), as follows:

$$\gamma^2 = -\left[\omega^2 L_R C_R + \frac{1}{\omega^2 L^2 \cdot L_{\text{total}} C_{\text{total}}} - \left(\frac{L_R}{L \cdot L_{\text{total}}} + \frac{C_R}{L \cdot C_{\text{total}}}\right)\right] \tag{10}$$

The phase constant is expressed as follows:

$$\beta = -j\gamma = s(\omega)\sqrt{\omega^2 L_R C_R + \frac{1}{\omega^2 L^2 \cdot L_{\text{total}} C_{\text{total}}} - \left(\frac{L_R}{L \cdot L_{\text{total}}} + \frac{C_R}{L \cdot C_{\text{total}}}\right)} \tag{11}$$

where

$$s(\omega) = \left\{ \begin{array}{ll} -1, & \omega < \min(\omega_{\text{se}}, \omega_{\text{sh}}) \\ +1, & \omega > \max(\omega_{\text{se}}, \omega_{\text{sh}}) \end{array} \right\} \tag{12}$$

are series and parallel resonances, respectively. Therefore, when the frequency is less than that of the series and parallel resonances, the unit material has left-handed characteristics. Actually, by banding up a pole to a ring with the bottom pole enclosed, this basic structural component becomes a kind of continuous topological change from a common parallel capacity.

For the left-handed structure, the serial body is mainly capacitive, and the parallel body is mainly inductive. According to the equivalent circuit diagram (Fig. 4), the magnetic resonance frequency of the C-shaped ring determines the region of negative permeability. The electrical resonance frequency determines the region of negative permittivity. Mutual coupling provides more adjustable factors for the structure and expands the scope of applications. The resonant frequency is defined by the following equation:

$$f = \frac{1}{2\pi\sqrt{L_{\text{total}} C_{\text{total}}}} \tag{13}$$

### 2.3. Performance Analysis

The value of $R_1$ is initially defined as an operating frequency set at 5.5 GHz; then, the other dimensions are derived according to Eq. (2), Eq. (4), and Eq. (13). Because the geometric dimensions of the designed unit (See Table 1) are not accurate, they are adjusted on the simulation software HFSS to meet the requirement for considering the unit material as a uniform medium. Simulation analysis of the designed unit provides the scattering $S_{11}$ and $S_{21}$ parameters, with a resonance point of 5.23 GHz (See Fig. 5).

| $L$ | $R_1$ | $R_2$ | $R_3$ |
|---|---|---|---|
| 10.00 | 3.30 | 2.80 | 2.30 |
| $w$ | $g$ | $h$ | $h_1$ |
| 0.50 | 0.25 | 0.50 | 6.50 |

**Table 1.** Geometric dimensions of the designed unit (in units of mm).

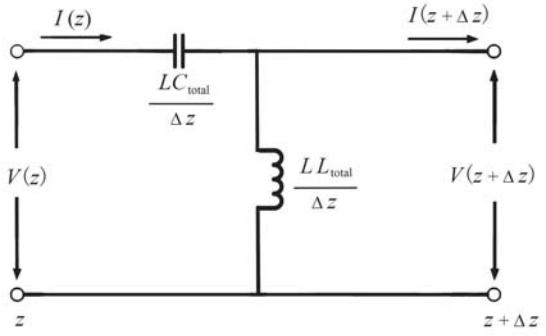


**Figure 4.** Transmission line circuit model of the C-shaped LHM.

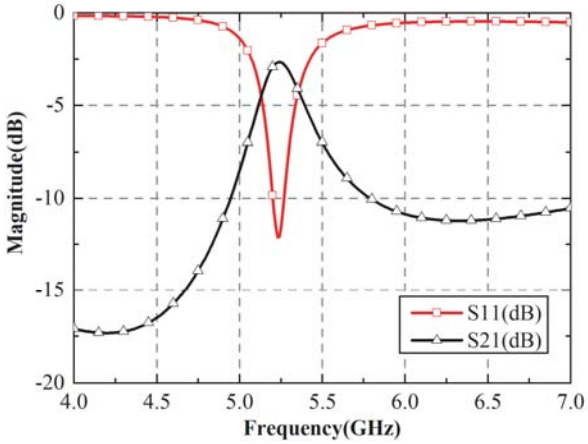


**Figure 5.** Simulated $S_{11}$ and $S_{21}$ parameters of the designed unit.

Using the equivalent parameter extraction method and MATLAB, the electromagnetic parameters of the designed C-shaped unit are obtained (See Fig. 6). From Fig. 6(a) and Fig. 6(b), it can be judged that the negative permeability band is $5.12 \sim 5.41$ GHz, with a very wide negative permittivity band of $4.0 \sim 7.0$ GHz. Therefore, it can be concluded that the left-handed band for the designed unit is $5.12 \sim 5.41$ GHz; whereas, the band of negative refractive index (NRX) is $4.4 \sim 6.0$ GHz (See Fig. 6(c)). Obviously, the bandwidth of NRX is significantly higher than that of DNCs, because NRX is derived as follows:

$$\mathrm{Re}(\varepsilon) \cdot \mathrm{Im}(\mu) + \mathrm{Im}(\varepsilon) \cdot \mathrm{Re}(\mu) < 0 \tag{14}$$

The condition may still be satisfied when only either permittivity or permeability is negative; thus, the NRX is insufficient to prove that the material has left-handed properties. The FOM, shown in Fig. 6(d), indicates the quality factor of the designed unit material. The higher the FOM, the smaller the loss of the material. As seen from Fig. 6(d), the FOM at the resonance point is also the highest point in the nearby frequency band.

For LHMs, the analysis using graphical topology alone is not sufficient to explore the effects and mechanism of modifications. Some of the graphic branches may be redundant during the design process, so the current flow distribution and the electromagnetic field pattern are needed to assist the analysis. Fig. 7 displays the pattern of the electromagnetic field and distribution of surface current for the unit structure. From Fig. 7(a), it is seen that the electric field is concentrated at the opening of the C-shaped ring. The presence of the circular patch widens the field distribution. At the same time, the electric field of the ideal electrical wall is almost zero (see Fig. 7(b)), which is consistent with the electrical boundary setting of the Perfectly Matched Layer (PML). It is seen from Fig. 7(c) that a reverse magnetic field is

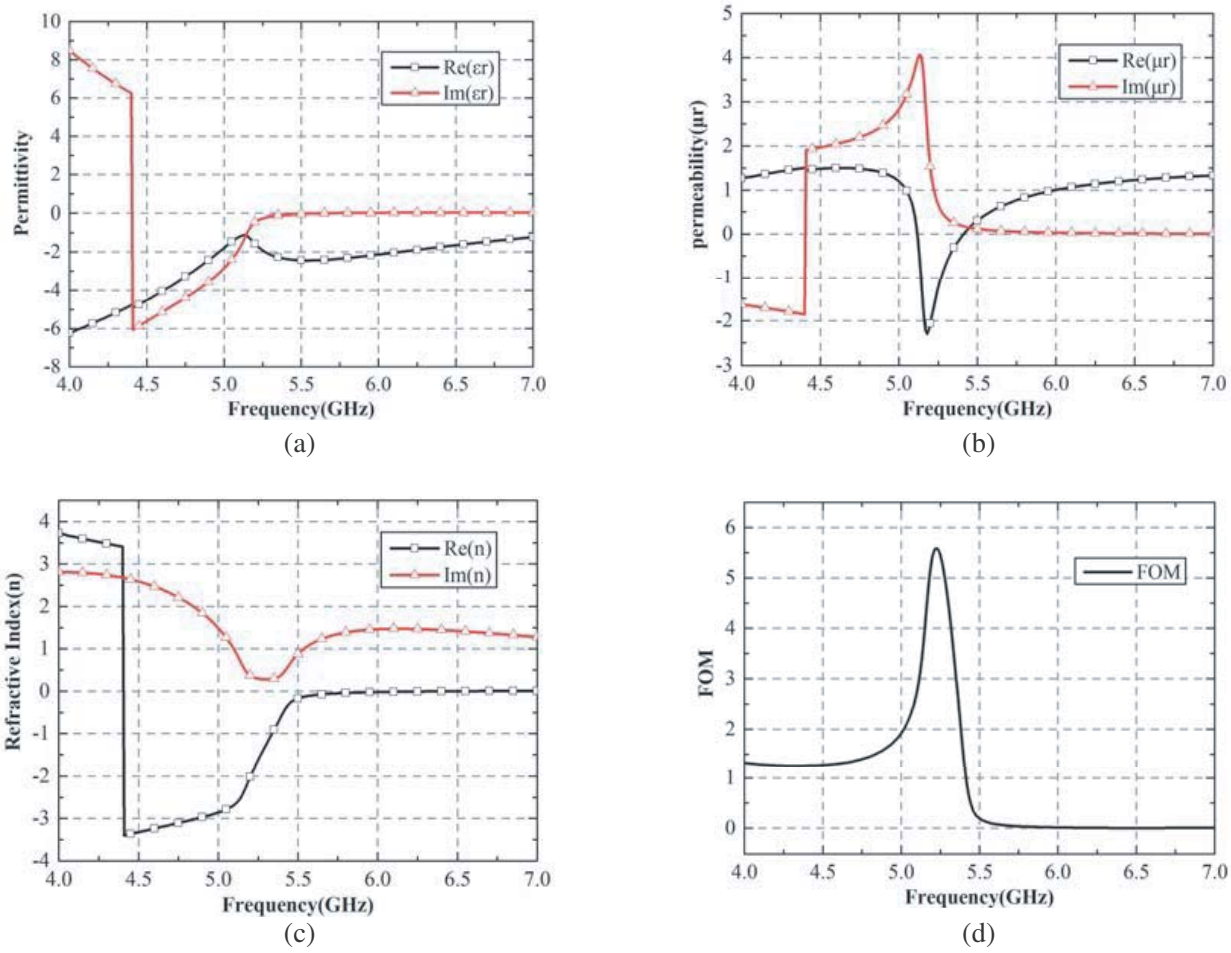


**Figure 6.** Extracted equivalent electromagnetic parameters of the designed C-shaped unit. (a) Permittivity, (b) permeability, (c) refractive index, (d) FOM.

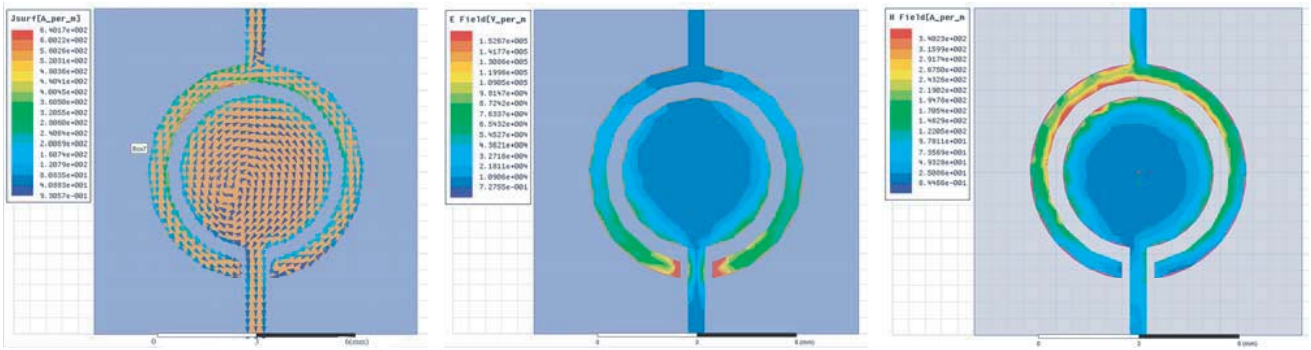


**Figure 7.** Simulated distributions of the designed C-shaped unit. (a) Current flow, (b) electric field strength, (c) magnetic field strength.

generated, where the topological change should be concentrated, due to the existence of the C-shaped ring. In a word, the circular C-shaped structure is a topology of a series capacitor and a parallel inductor. The equivalent electromagnetic characteristics of the modified structural units, through three kinds of topology deformations, are to be expected.

### 2.4. Topological Deformation and Analysis

The principle of differential and homeomorphic topology deformation is to adjust the performance of a graph to a certain extent without changing the topological structure of the graph and the overall trend of the current distribution. First of all, a simple topological change is made to the proposed unit (See Fig. 8) by loading a gear-shaped structure with an interlaced layout of many small rectangular patches between the C-shaped ring and the circular patch. The flow length of the current is effectively enhanced by loading the gear structure. Simultaneously, the length of the inductor becomes longer, and the inductance value increases; whereas, for the capacitor, the distance between the capacitor sheets is reduced, and the capacitance increases. As seen from Eq. (5), the resonant frequency is reduced so that, with the same radius, the deformed unit has a larger equivalent electric-length, which means that there is an obvious possibility for the miniaturization of the designed unit structure.

| $L$ | $R_1$ | $R_2$ | $R_3$ |
|---|---|---|---|
| 7.00 | 3.00 | 2.50 | 2.00 |
| $w$ | $g$ | $h$ | $h_1$ |
| 0.50 | 0.25 | 0.50 | 6.50 |

**Table 2.** Geometric dimensions of the deformed unit (in units of mm).

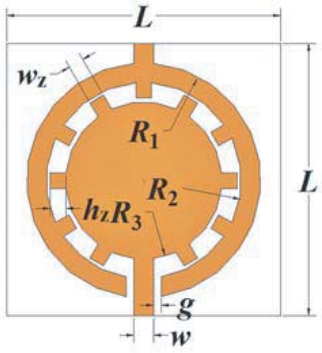


**Figure 8.** Configuration of the deformed gear-like unit structure.

To maintain the distributions of the electromagnetic fields and the direction of the current, the difference, $d$, between the inner and outer radii of the C-shaped ring and the distance, $d_1$, between the C-shaped ring and the circular patch remain constant during the design. Through simulation analysis of the deformed unit, it is found that, by decreasing $R_1$, the reduced resonant frequency shifts to the right, with final dimensions as listed in Table 2. The overall size is thirty percent smaller than that of the original C-shaped ring structure. The internal ring structure size is ten percent smaller. Simulated scattering parameters of the deformed gear-shaped unit, compared with that of the original C-shaped unit, are plotted in Fig. 9. According to the calculated equivalent permittivity and permeability (See Fig. 10), the DN frequency band of $5.11 \sim 5.57$ GHz is wider than that of the original unit. Concurrently, the loss is reduced due to the smaller size of the inner circular patch, which means that the deformed structure has certain FOM improvement characteristics. Therefore, by loading the gear-like structure without damaging the performance, the left-handed unit structure is miniaturized to make additional space for more structural loading. Because the structure body changes in length only with the connection or fracture characteristics unchanged, this is a continuous homeomorphic change. The circuit body is still comprised of a series capacitor and a parallel inductor, with only value changes for capacitance and inductance. Combined with the variations of electromagnetic parameters, the natural performances also change continuously, and the resonant frequency shifts. Based on topology theory, compared with the original circular-C-shaped unit, the deformed gear-like unit has no change in the pattern topology. The prominent gear is therefore called an elastic change in the topology, and, on one hand, its extrusion is restored to the original structure. On the other hand, because this change is only a process of continuously extending the reactance change, the changed gear shape remains the bilateral symmetry characteristic of the original structure.

The homeomorphic topology deformation of the circular patch, with certain inheritance to the original structure, is proposed as shown in Fig. 11(a). However, the original symmetrical configuration is changed to an asymmetric configuration, thereby modifying the performance of the unit. For simulation analysis, the length of the bending rectangle is set at 2 mm and the bending degree set at 135°, keeping

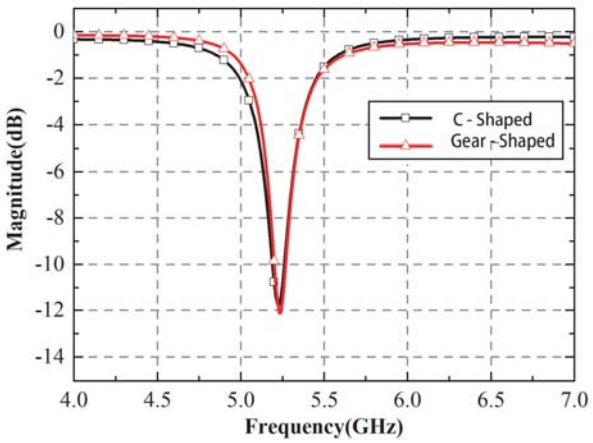


**Figure 9.** Comparison of the simulated $S_{11}$ for the deformed gear-shaped unit and original C-shaped unit.

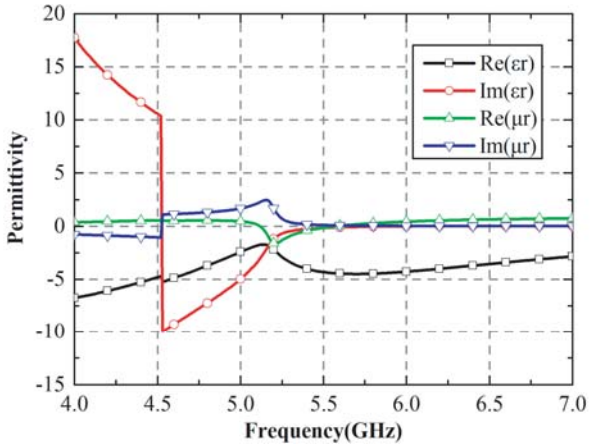


**Figure 10.** Double negative characteristics of the deformed gear-shaped unit.

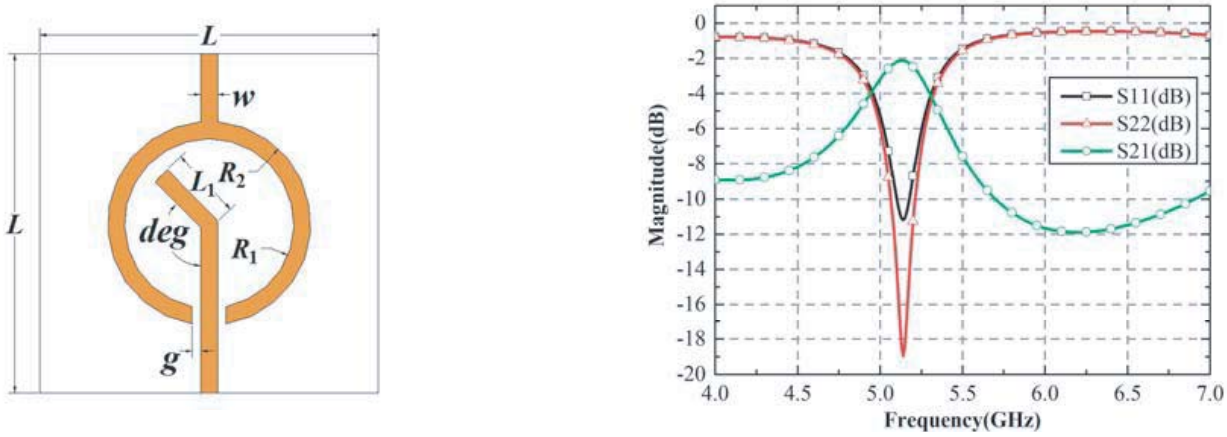


**Figure 11.** Deformed Clock-shaped unit. (a) Configuration, (b) $S$-parameters.

the other dimensions and substrate parameters unchanged. According to the simulation results (See Fig. 11(b)), it is found that the resonance point is at 5.15 GHz. Referring to a typically asymmetric structure, the simulated values of the $S_{11}$ and $S_{22}$ parameters of the deformed unit are unequal. The simulation results (See Fig. 12(a) and Fig. 12(b)) are obtained through data processing. The equivalent permeability and permeability are negative from 4 GHz to 7 GHz and from 5.00 GHz to 5.44 GHz, respectively; therefore, the double negative band is $5.00 \sim 5.44$ GHz. From topology theory, the deformed clock-shaped structure, with the similar topology maintained, can still be considered as an elastic change of the original Circular-C-shaped structure. As mentioned in Section 1, this is a homeomorphic deformation of the topological structure. In the deformation design, with the shape length varying greatly, there is no change in the fracture or joint parts. The corresponding circuit characteristics are only the capacitance-inductance values. The electromagnetic parameters are continuously changed. However, compared with the original C-shaped structure with left-right symmetry, the deformed clock-type structure does not have a symmetrical characteristic, which changes the bilateral symmetry of the topology. In conclusion, the changes in the nature of the graphical topology result in the variations in the electromagnetic parameters.

For homeomorphic topological deformation, it is possible to produce performance modifications

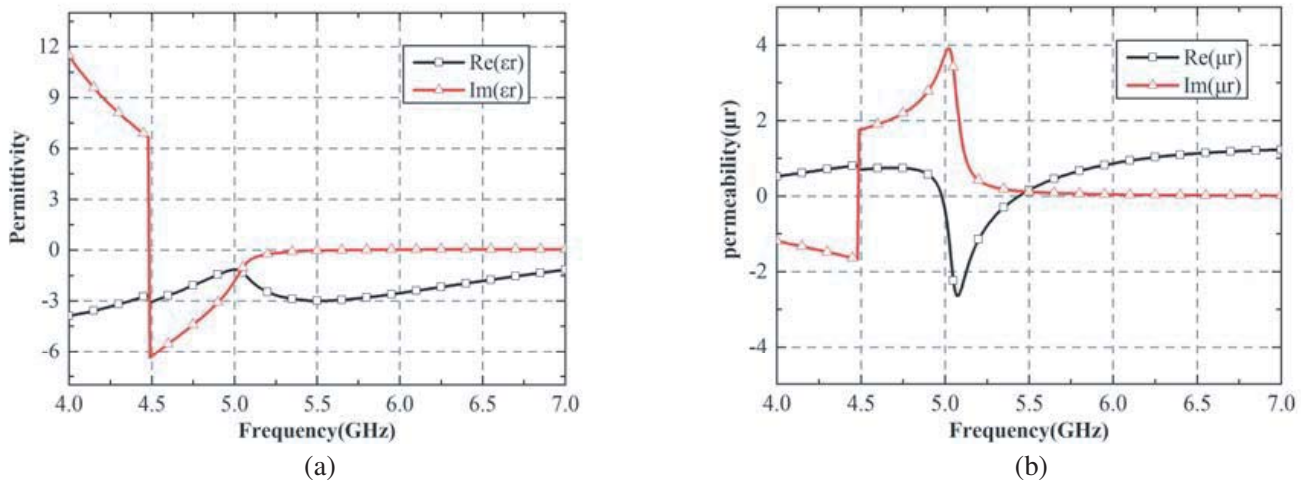


**Figure 12.** Equivalent electromagnetic parameters of the deformed Clock-shaped unit. (a) Permittivity, (b) permeability.

while retaining some, or most of, the original characteristics, which is very useful for improving LHMs. When the current and electromagnetic field distributions of a LHM are known, homeomorphic topology deformation is made on the basis of the maintenance of the original distribution and orientation, with an adjustment in the overall performances. Concurrently, symmetry in the original configuration is adjusted. The change of the derivative loop makes it possible to realize a parasitic left-handed band and obtain a double-pass left-handed structure.

The non-homeomorphic topological deformations of the left-handed structure refer to herein coincidence, splitting, and cyclic transformations, dividing the original into multiple parts, or integrating multiple parts, of the connection into one part. The properties of the new structure obtained by such a deformation vary widely and are rarely the same as the original ones. For example, if the C-shaped ring is disconnected from the middle part, the structure will have no left-handed characteristic. However, for some unit structures without left-handed characteristics, the left-handed characteristics may be generated by special processing, such as breaking or connecting. As shown in Fig. 13(a), based on two large C-shaped structures up and down, the left and right ends, respectively, are connected with a small C-ring and a circular patch. To generate a negative permittivity, the intermediate fracture is transformed into a metal rod, and the two large C-structures are coupled to form a larger loop circuit. Combined with the topological analysis, the internal fracture of the internal transmission line is divided into two lines. Also, induced capacitance occurs between the two lines, which are equivalent to a sensor arm. The outer rings, at the left and right sides, are also broken into two segments to simultaneously generate capacitance and inductance. The lower side changes from the original fracture to the junction. This is just a non-homeomorphic topological deformation with variations in properties, while the structural patterns discontinuously change and the electromagnetic properties vary significantly. An equivalent circuit diagram is made according to the unit pattern combined with the left- and right-handed transmission line theory (See Fig. 13(b)). After the non-homeomorphic deformation, a shunt capacitor, $C_2$, appears in the parallel branch, and a series inductor, $L_1$, appears in the series branch. If the equivalent capacitance and the series inductance play a major role, the model has no left-handed characteristics. The left-handed characteristics in a specific frequency band are achieved by adjusting the capacitance and inductance of the equivalent circuit. Thus, non-homeomorphic topological deformation, with a major turning point for the electromagnetic characteristics, may lead to the performance transformation of the unit structure from a left-handed feature to a right-handed feature.

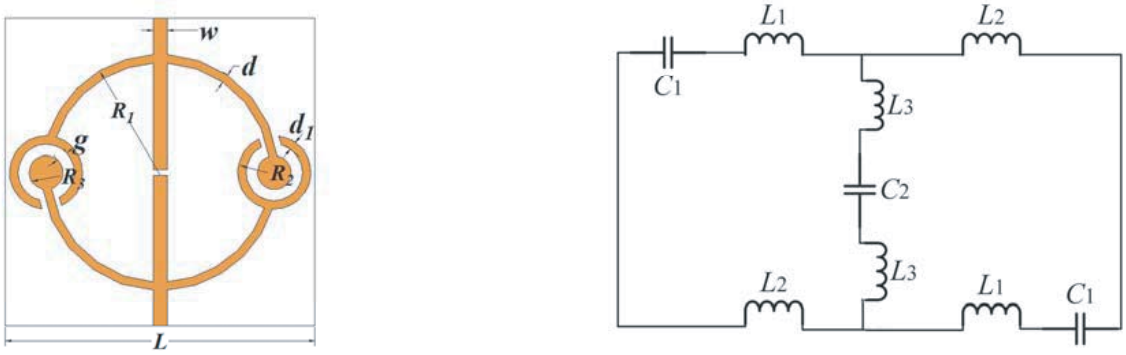


(a) (b)

**Figure 13.** Circular-C-shaped cyclic coupling unit. (a) Configuration, (b) equivalent circuit diagram.

## 3. DESIGN OF ANTENNAS

### 3.1. Left-Handed Structural Unit

According to the analysis of the circular-C-shaped ring and relative topology deformations, those coupling structures contribute to the generation of capacitance. The circular C-shaped structure,

| $L$ | $R_1$ | $d_1$ | $d_2$ |
|---|---|---|---|
| 10.00 | 3.30 | 0.50 | 0.50 |
| $w$ | $g_c$ | g | $L_1$ |
| 0.50 | 0.40 | 0.50 | 3.20 |

**Table 3.** Geometric dimensions of the handshake-shaped unit (in units of mm).

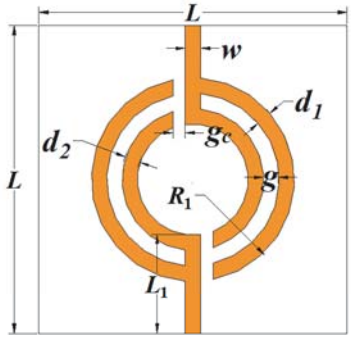


**Figure 14.** Configuration of the deformed initially handshake-shaped unit.

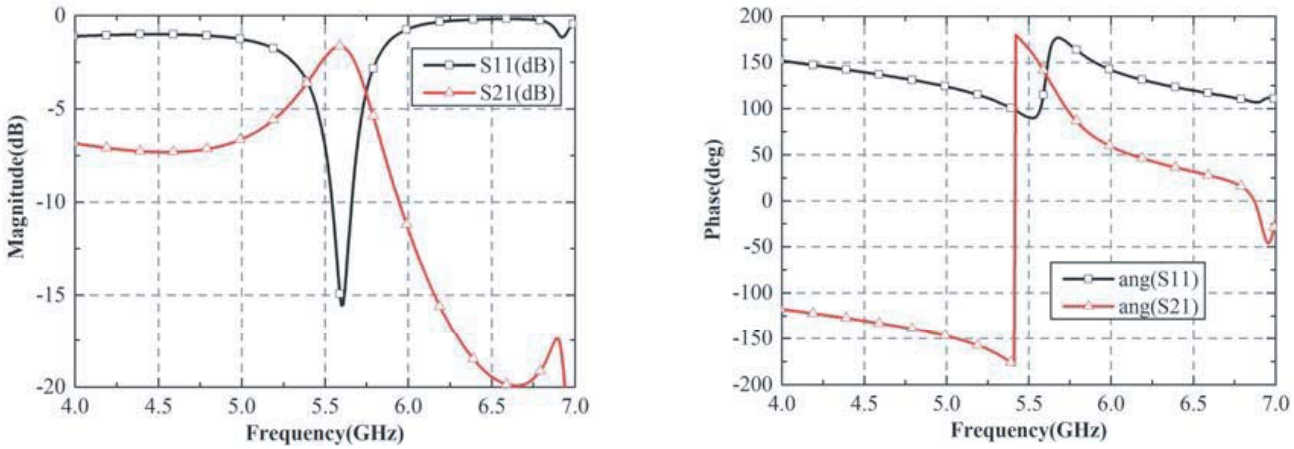


(a) (b)

**Figure 15.** Simulated $S_{11}$ and $S_{21}$ parameters of the handshake-shaped unit. (a) Amplitude, (b) phase.

originally established in this paper, is the simplest left-handed structure, which is convenient for topological idea analysis. However, the performance is ordinary. To improve antenna performance, we carried out the non-homeomorphic topology change of the original circular C shape. Combined with the three topological changes mentioned above, it is seen that the original circular-C-shaped ring is now topologically transformed into a semi-circular U-shaped ring to form a handshake-shaped LHM unit (See Fig. 14). Actually, the unit structure is a reverse sleeve of the original. The middle portion divides the originally connected inductance into two segments and introduces a series inductor to facilitate the increase of left-hand characteristics. The middle part separates into upper and lower parts, with the right part connected to the outer ring. The left half of the outer ring is broken and connected, and the series capacitance of the lower half is transferred to the upper half to realize an asymmetric structure, which may generate a second resonance point. This is a non-homeomorphic topological deformation through fractures and connections, with an abrupt change in pattern structure and electromagnetic properties. To maintain the LHM characteristics, the two-section transmission line is placed left and right to the semi-circular, resulting in a series capacitance. The double loop structure is perpendicular to the incident magnetic field and generates a negative permeability. A coupled capacitor is formed between the large and small rings, which increases the total capacitance and, therefore, may enhance the left-handed characteristics. Each small element of the handshake-shaped unit can be regarded as a curved U-shaped ring; thus, there is a possibility that a second type of resonant loop is generated. Taking 5.5 GHz as the design frequency point, preliminary dimensions (See Table 3) were calculated

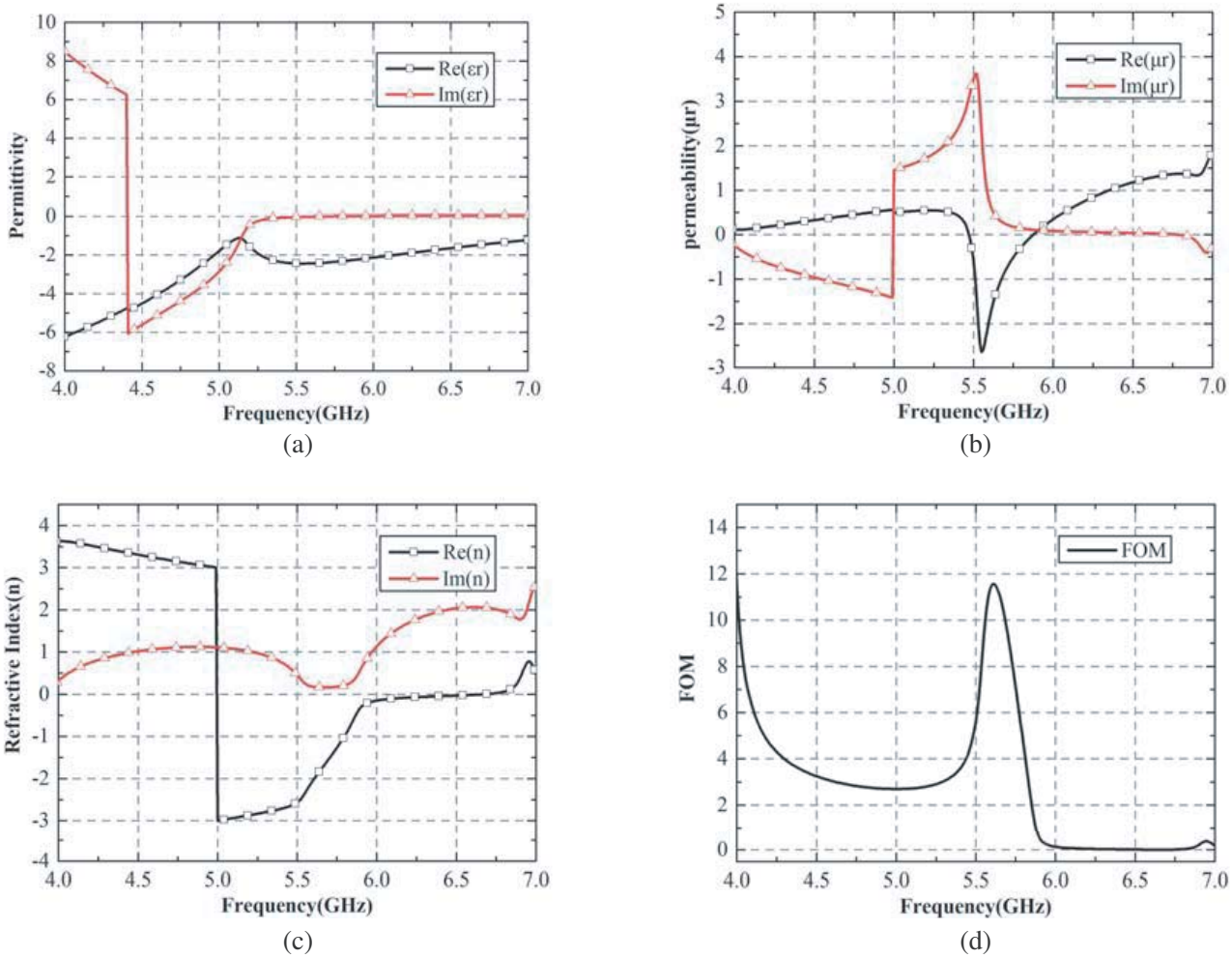


**Figure 16.** Equivalent electromagnetic parameters of handshake-shaped unit. (a) Permittivity, (b) permeability, (c) refractive index, (d) FOM.

and briefly adjusted.

According to the simulated $S_{11}$ and $S_{21}$ values of the handshake-shaped unit as plotted in Fig. 15, the electromagnetic parameters are extracted as shown in Fig. 16. The equivalent permittivity is negative in the frequency band above 4.06 GHz, and the equivalent permeability is negative in the frequency band of $5.47 \sim 5.88$ GHz. Therefore, the frequency band with the left-handed characteristic is $5.47 \sim 5.88$ GHz. However, after non-homeomorphic topological deformation, the unit pattern changes from the original symmetrical structure to an asymmetric one. The electromagnetic parameters also exhibit asymmetrical characteristics. Mutation of the topology causes the electromagnetic properties to transform from right-handed to left-handed characteristics. Also, there may be two resonant circuits in the structure. Each of the hand branches has a curved U-shaped loop. The whole unit is used as a large open loop; consequently, there is the possibility of dual-band improvement.

To expand the structural performance of the handshake-shaped unit, an annular line is added inside the semi-circular U-shaped hand to form the overall alternately coupled annular unit structure (See Fig. 17). There are broken, connected, and added mutations in the topology, and the series inductance in the middle part of the original structure is changed to a series capacitor. Furthermore, the upper part of the outer ring increases the series capacitance to realize left-handed characteristics. A loop line is added to increase the coupling; thus, to increase capacitance value, the spacing between the two plates of the induction capacitor are reduced. The upper and lower portions of the loop line, with a series capacitor introduced, are in an off-state. A coupling between the loop lines, along with changes in the topology, may also produce new resonance points. The intermediate annular layer enhances the resonance of the curved U-shaped loop, which is not connected to it. Because the three-layer coupling structure is much more complicated, the size of the whole unit must be larger than that of a handshake-shaped structure. Correspondingly, the resonant frequency of the ring circuit decreases. To better adapt to the 5G mid-band communication, the resonance frequency of the loop is adjusted to the 3.5 GHz band. The dimensions are calculated and briefly adjusted (See Table 4).

According to the simulated $S_{11}$ and $S_{21}$ values of the overall alternately coupled annular unit, as plotted in Fig. 18, the resonance points are at 3.57 GHz and 5.64 GHz. After the intermediate loop is loaded for mutual coupling, the second resonant frequency is highlighted. As seen in Fig. 19(a) and Fig. 19(b), for the extracted equivalent permittivity and permeability, the double negative frequency bands are $3.44 \sim 3.71$ GHz and $5.63 \sim 6.50$ GHz, respectively, which are slightly narrower than those of the calculated equivalent refractive index (See Fig. 19(c)). As shown in Fig. 19(d), the FOM values, at 3.57 GHz and 5.64 GHz, are 9.44 and 35.7, respectively. Visible loss is significantly reduced, and, compared with the handshake-shaped unit, overall performance is greatly improved. The discontinuous change of the structure, combined with the influence of non-homeomorphic deformation, causes discontinuity in the electromagnetic parameters; therefore, the electromagnetic parameters are abrupt, and multiple frequency points appear.

| $L$ | 11 | $h_1$ | 1.6 |
|---|---|---|---|
| $R_1$ | 5.0 | $g_1$ | 0.30 |
| $g_2$ | 0.30 | $g_3$ | 0.20 |
| $g_4$ | 0.20 | $d_1$ | 0.40 |
| $d_2$ | 0.40 | $d_3$ | 0.40 |
| $W_1$ | 0.40 | $W_2$ | 0.20 |

**Table 4.** Geometric dimensions of the interactive coupling annular unit (in units of mm).

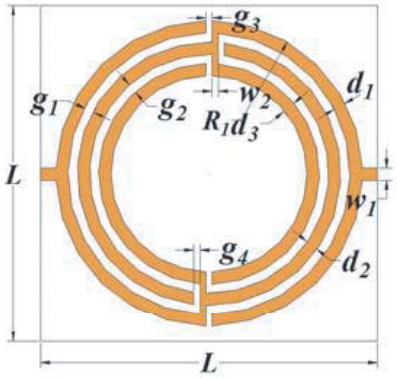


**Figure 17.** Configuration of the overall interactive coupling annular unit.

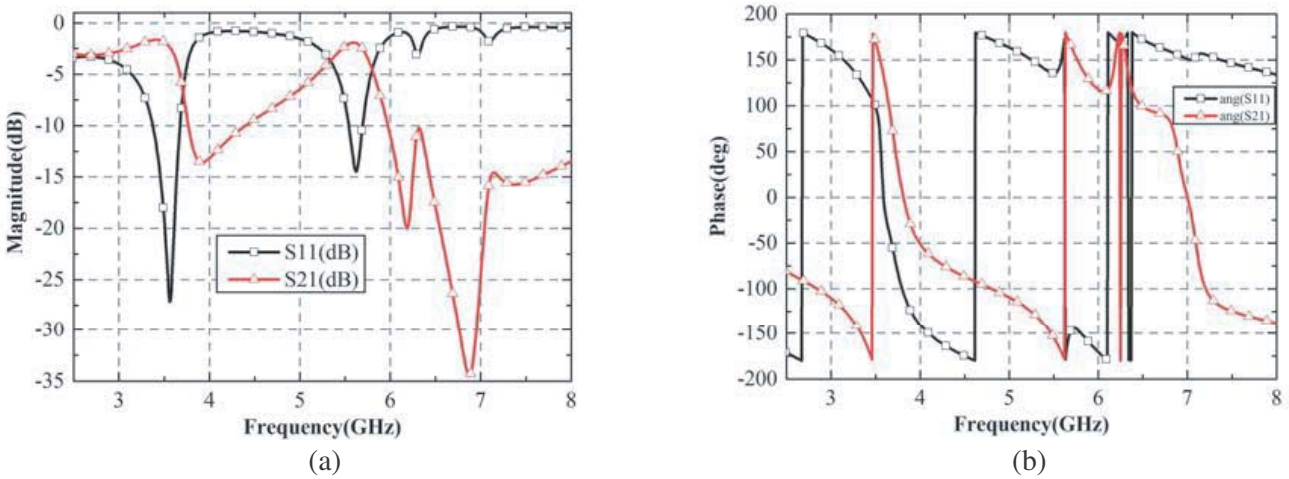


**Figure 18.** Simulated $S_{11}$ and $S_{21}$ parameters of the overall interactive coupling annular unit. (a) Amplitude, (b) phase.

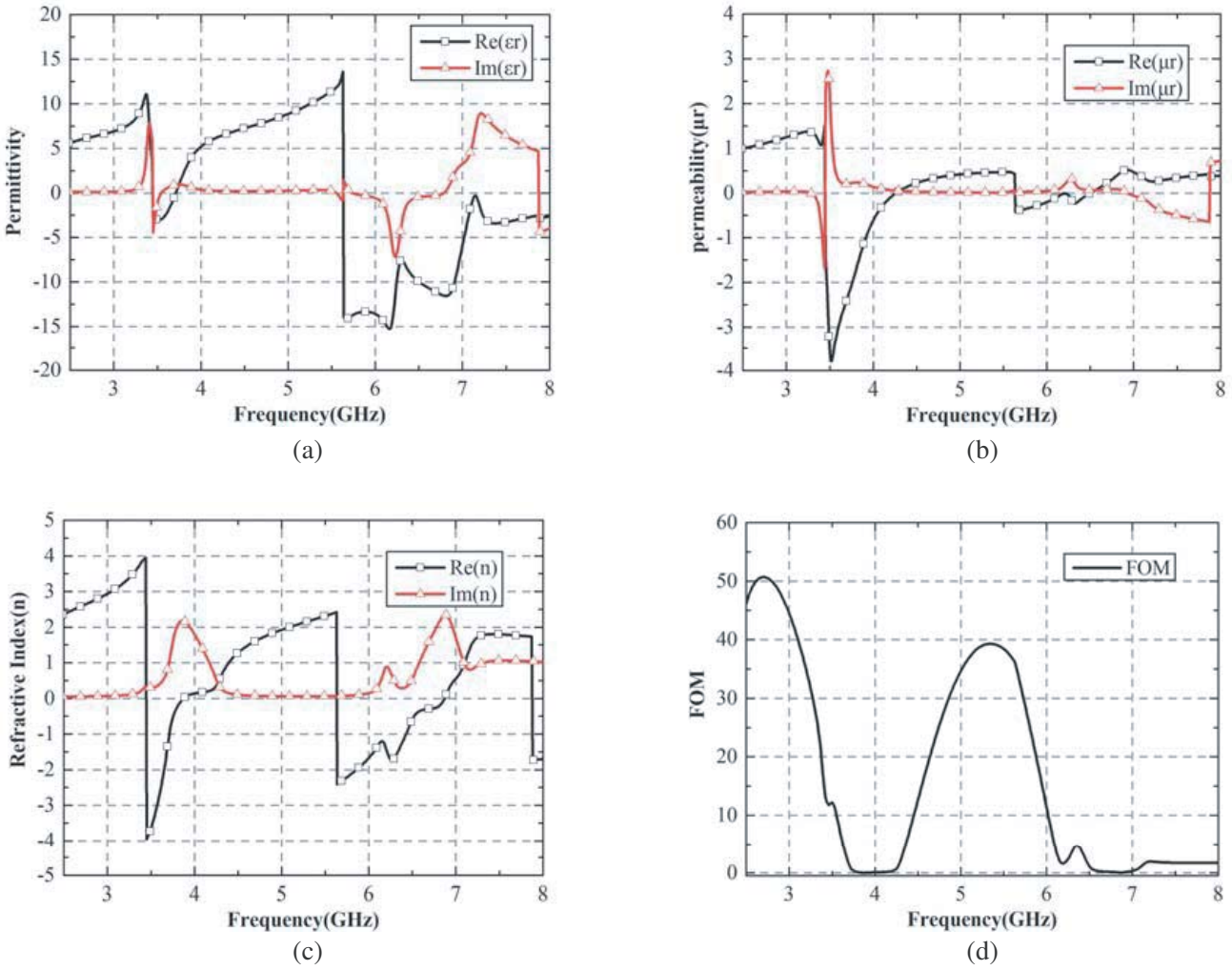


**Figure 19.** Equivalent electromagnetic parameters of the overall interactive coupling annular unit. (a) Permittivity, (b) permeability, (c) refractive index, (d) FOM.

### 3.2. Ultra-Wideband Antenna Combined with LHMs

First of all, as shown in Fig. 20(a) and Fig. 20(b), a microstrip monopole ultra-wideband antenna is designed. The upper layer of the basic UWB antenna adopts a circular patch. The lower floor is in the form of a rectangle under a semi-ellipse with a rectangular slot opened therein to further expand its bandwidth.

From the simulated $S_{11}$ values, depicted by the red line in Fig. 22, it is seen that for the basic antenna, without loading any LH unit, but only changing the grounding plate, an ultra-wideband characteristic is achieved with a reflection coefficient of less than $-10$ dB over the frequency range of 2.39 $\sim$ 17.7 GHz. The bandwidth reaches 15.31 GHz, and the relative bandwidth reaches 152%, indicating good broadband performance. To prevent any interference to antennas applied in the communication systems, it is necessary to design the notch characteristics of the antenna in some frequency bands. Considering notch ability, a left-handed unit structure, with a complementary ring, is dug into the circular patch on the upper layer of the basic antenna to form a gap (See Fig. 21). The resonance ring of the loaded LH unit is used to realize the interference of the current, thereby, realizing the notch effect. The optimized dimensions of the loaded LH unit are listed in Table 4.

From the simulated $S_{11}$ values, depicted by the black-line in Fig. 22, it is found that a new resonant gap, mostly affected during the range of 2.5 $\sim$ 5 GHz, is formed inside the antenna. As can be seen from Figs. 19 (a), (b) and Fig. 22, the LHM properties of the center-loaded left-handed unit are abruptly changed around 3G and 5G frequencies. Correspondingly, the $S_{11}$ parameter is also changed under

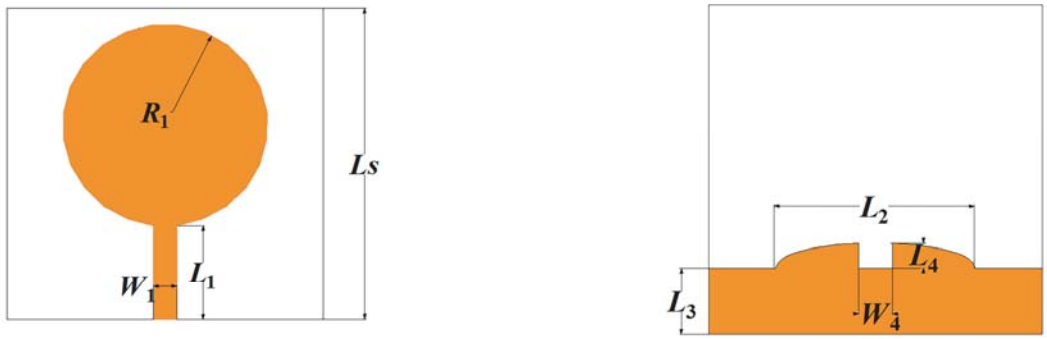


**Figure 20.** Configuration of the basic UWB antenna. (a) Upper layer, (b) lower floor.

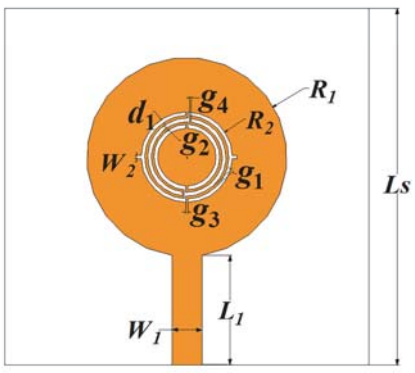


**Figure 21.** Configuration of the designed UWB antenna with a LH unit loaded on the upper layer.

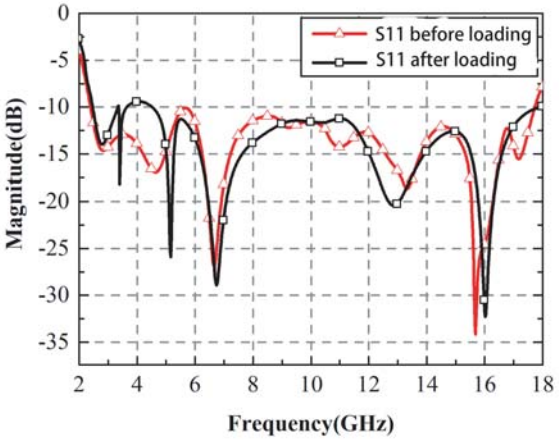


**Figure 22.** Simulated $S_{11}$ parameters of the designed UWB antenna before and after loading LH unit.

the control of the left-hand unit around 3G and 5G. The trapping function is realized by the anomaly local control overall the design. This coincides with the double negative frequency band of the loaded LH unit, which is speculated as large interference near the band. Thus, a notch frequency band of 3.62 $\sim$ 4.54 GHz appears, with a notch bandwidth of 920 MHz. Compared with traditional notch antennas, the notch band of the designed UWB antenna is wider, with bright prospects of application.

For the UWB antenna without loading an LH gap, to realize the radiation, the current is generally concentrated outside the patch, with the distribution at the edge of the circle and the feed. The simulated current distributions at three resonant frequency points of the designed UWB antenna with the LH unit loaded are displayed in Fig. 23(a), Fig. 23(b) and Fig. 23(c). After loading the LH unit, the current is concentrated inside the left-handed gap at the resonance frequency.

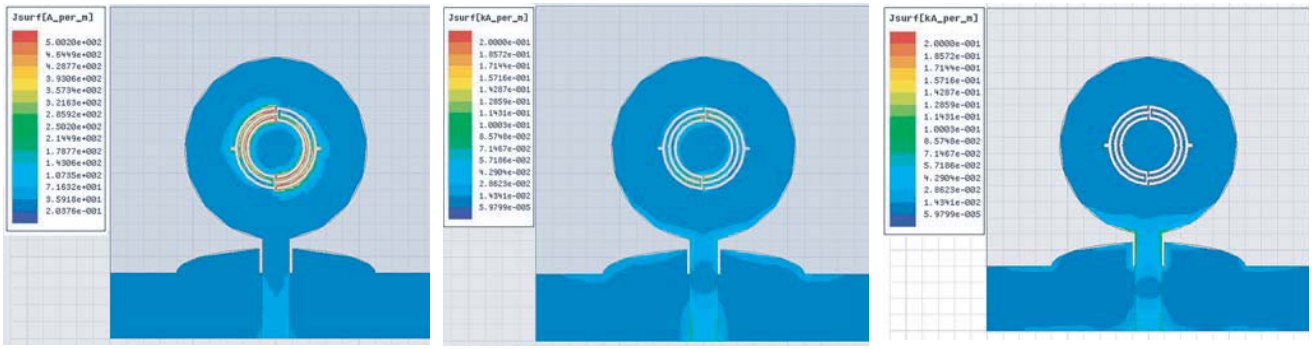

(a) (b) (c)

**Figure 23.** Current distributions of the designed UWB antenna with the LH unit loaded at (a) 3.40 GHz, (b) 5.16 GHz, (c) 6.74 GHz.

For the lower operating frequency near the resonance point of the LH unit (about 3.40 GHz), the current is concentrated inside the left-handed gap. The current concentrated in the gap weakens the outside current, thereby, reducing the radiation at the double negative resonance point and generating strong notch characteristics. But for the higher frequency bands that deviate from the resonance point of the LH unit, such as 5.16 GHz and 6.74 GHz, so as not to interfere with the operating characteristics, the current is not disturbed. Therefore, the introduction of the left-handed slot into the designed UWB antenna achieves the performance of limiting the current distribution in a specific frequency band. Since the characteristics of the left-handed unit are often known before loading, notching can be targeted with obvious features.

### 3.3. Improved UWB-MIMO Antenna with Loading LH Gaps

By virtue of its high bandwidth, a UWB antenna achieves a large data throughput rate, and that advantage is further enhanced by the combination with MIMO technology. To reduce the isolation of the two unit structures, a left-handed unit is added as an intermediate separation strip. Two LH elements, with complementary rings, are loaded onto the upper layer of a two-unit MIMO antenna (See layout in Fig. 24). According to the above analysis, the LH slot dug inside a UWB antenna exists as a notch unit. Then, to act as an electromagnetic bandgap, three connected Circular-C-shaped cyclic coupling LH elements are introduced in the middle of the MIMO antenna.

According to the designed UWB-MIMO antenna, a prototype is fabricated on an FR4 substrate and analyzed by a vector network. In Fig. 25, several photos of the fabricated antenna are displayed as follows: front view and back view before loading the LH bandgap shown in Fig. 25(a) and Fig. 25(b), respectively; as front view and back view after loading the LH bandgap shown in Fig. 25(c) and Fig. 25(d), respectively. Similar to the design, on the substrate there is a 0.02 mm thick copper layer with a relative dielectric constant of 4.4 and a loss tangent angle of 0.02. The dimensions of the UWB-MIMO antenna are listed in Table 5. For comparison, the simulated and measured $S_{11}$ and $S_{12}$ values are shown in Fig. 26(a), Fig. 26(b), Fig. 26(c), and Fig. 26(d). For the MIMO antenna

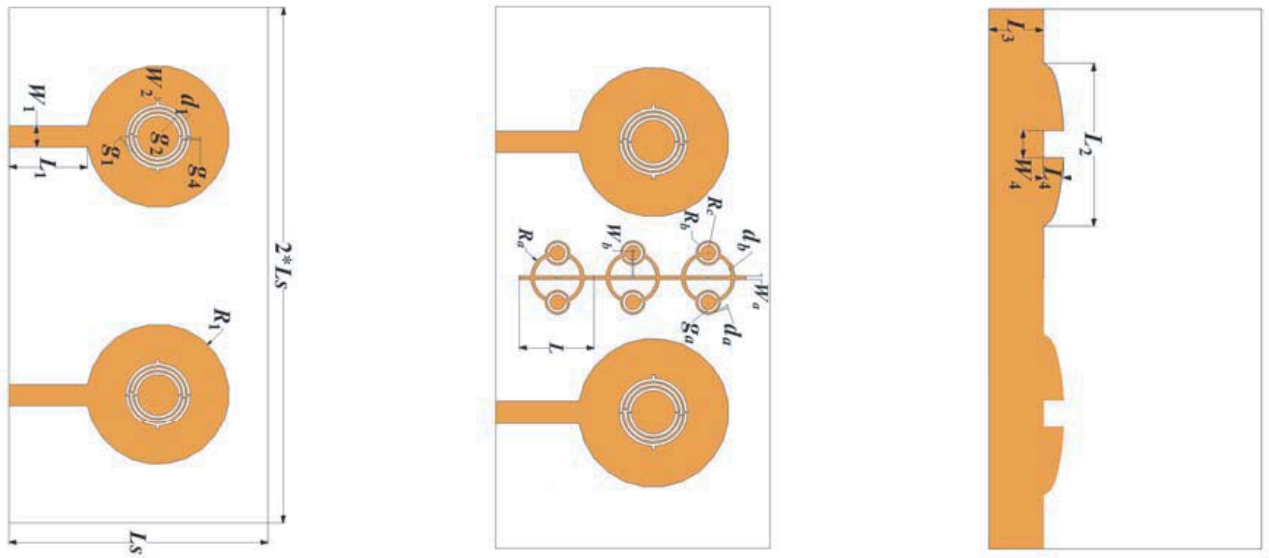


(a) (b) (c)

**Figure 24.** Configuration of the proposed UWB-MIMO antenna with two kinds of LH elements loaded. (a) Upper layer with two complementary rings, (b) upper layer with three connected coupling cycles, (c) lower floor.

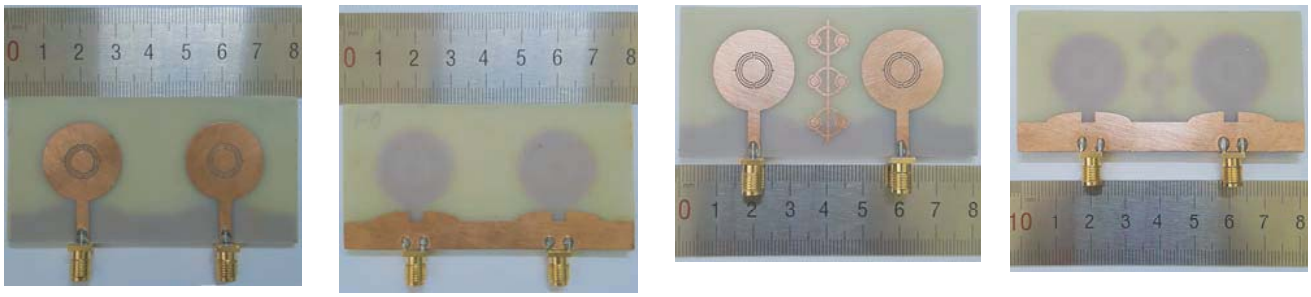

(a) (b) (c) (d)

**Figure 25.** Prototype photos of the designed UWB-MIMO antenna. (a) Front view before loading bandgap, (b) back view before loading bandgap, (c) front view after loading bandgap, (d) Back view after loading bandgap.

**Table 5.** Geometric dimensions of the interactive coupling annular unit (in units of mm).

| | | | |
|---|---|---|---|
| $R_a$ | 3.90 | $R_b$ | 1.80 |
| $R_c$ | 1.10 | $L$ | 11.0 |
| $W_a$ | 0.500 | $W_b$ | 0.200 |
| $d_b$ | 0.500 | $d_a$ | 0.300 |

without any LH bandgap loaded, according to the $S_{12}$ diagrams, the transmission coefficient in the passband range is mostly between $-10$ dB and $-15$ dB, indicating there is a high coupling between the two units. When the two antenna units work simultaneously, a large interference, which is not conducive to the stability of the antenna operation, occurs between them. However, antenna isolation is significantly improved after loading the LH bandgap. The most obvious frequency band is the double-negative one of the center-loaded circle-C-shaped LH unit; notch ability is also improved in

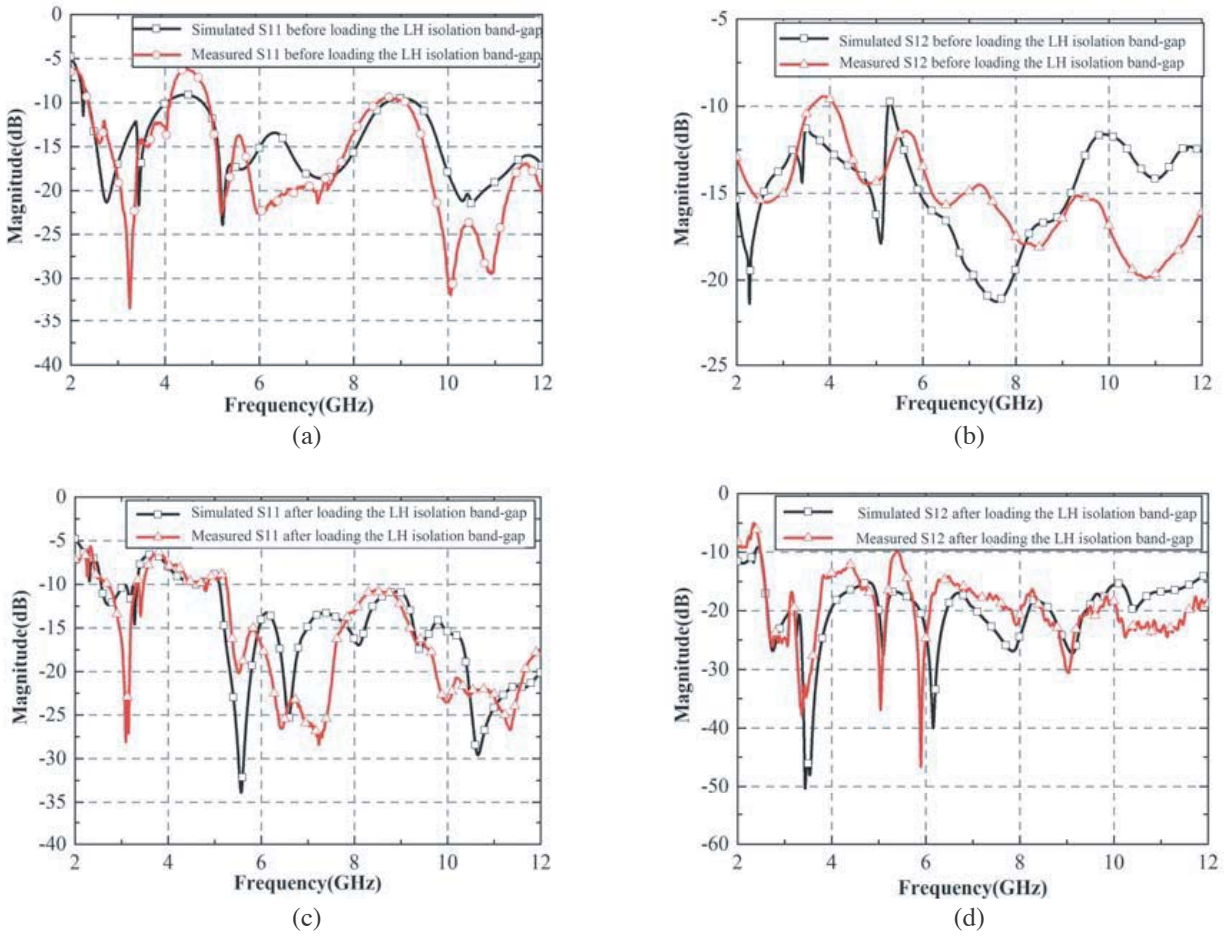


**Figure 26.** Measurement and simulation comparison of the designed UWB-MIMO. (a) $S_{11}$ values before loading bandgap, (b) isolation comparison before loading band-gap, (c) $S_{11}$ values after loading bandgap, (d) isolation comparison after loading band-gap.

this band. Below and above respectively, Fig. 27 shows the $S_{11}$ and $S_{12}$ parameters before and after loading the left-handed isolation strip. The middle part is the LHM characteristics of the isolation strip structure itself. It can be seen that the material properties are abrupt at the three frequencies, and the intrinsic properties of the isolation strip are abruptly changed from the right-handed characteristic to the left-handed characteristic. According to the $S$-parameters after loading the isolation strip, there is a change in the local equivalent material parameters between the antenna elements. The isolation is improved by localized anomalies that regulate the overall antenna performance. The phase change can be more flexibly obtained with CRLH structure in the limited space compared with conventional right-handed materials, thereby changing the electromagnetic characteristics. As a result, the CRLH structure improves the phase control of the loaded isolation strip and then the isolation performance. Finally, for this improved UWB-MIMO antenna, the interference is reduced to 5G, including 3300–3400 MHz, 3400–3600 MHz and 4800–5000 MHz bands. It can be seen from all the figures that the measured data before and after loading are consistent with the simulation data. The stop band is narrow before loading; the average isolation is about −15 dB. After loading the left-handed isolation bandgap, there is a stopband, with overall isolation about −20 dB, in the required suppression band. The radiation efficiency of the novel UWB-MIMO antenna reaches 90.38%, and the gain at the center of the main lobe is 5.7 dB.

Compared with other research works [23–25], with left- and right-handed composite structures, it is easier to implement flexible control. There are different isolation effects for different numbers of array elements. The diagrams of the corresponding antenna performances, when the number of array units

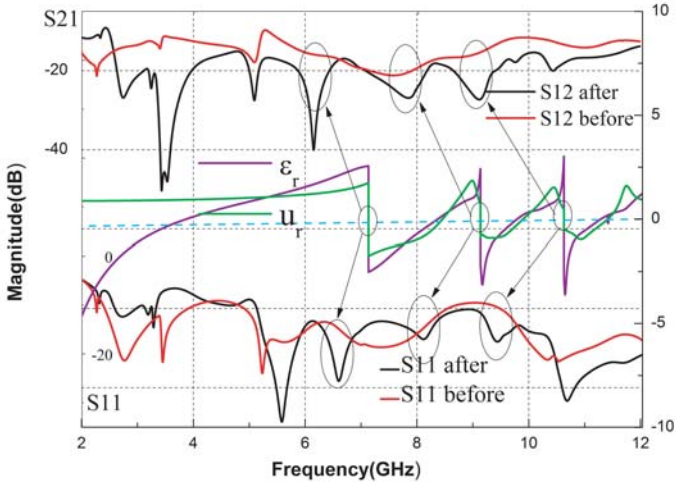


**Figure 27.** LHM characteristics of the loaded isolation bandgap and $S$-parameters after and before loading.

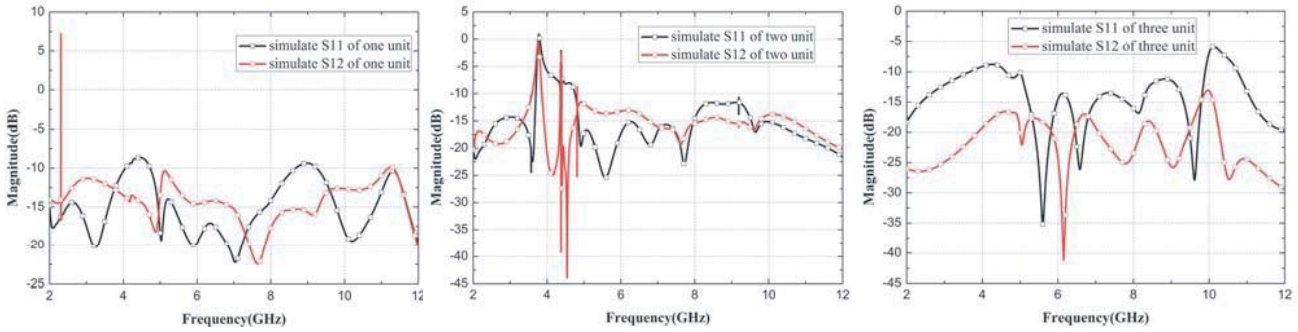


**Figure 28.** Simulated performances of the designed antenna after loading the proposed left-handed structure with (a) one unit, (b) two units, (c) three units.

is 1, 2 and 3, are shown in Fig. 28(a), Fig. 28(b), and Fig. 28(c), respectively. The simulation results show that, as the number of array elements increases, isolation performance is improved, which is closer to the left-handed structure performance in the periodic analysis originally in this paper. The designed antenna is mutated at 1.9 GHz, which may be caused by the structure of the loaded left-handed unit.

## 4. CONCLUSION

Based on an antenna unit, in combination with a circular C-shaped ring and an interaction ring, the influences of various topological changes on antenna performance and electromagnetic characteristics were analyzed in detail. The conclusion is that a change in the topology of an antenna structure is closely related to the performance of the antenna, and topological analysis is potentially important for antenna development.

For 5G communication, a novel UWB-MIMO antenna with an LH isolation bandgap and central-loading circle-C cycle LH units was designed, optimized, and measured. After loading the left-handed units, a notch band, with a notch bandwidth of 920 MHz, appears in the range 3.62 $\sim$ 4.54 GHz. Compared with conventional notch antennas, the antenna notch band is wider, and the application value is higher. Moreover, for this UWB-MIMO antenna, the interference, including 3300–3400 MHz, 3400–3600 MHz, and 4800–5000 MHz bands, is reduced to 5G. Overall isolation is about $-20$ dB in the range of the stopband, which is significantly improved to meet the practical requirements.

## REFERENCES


1. Hamidian, A. and V. Subramanian, "Right and left handed transmission lines for millimeter wave applications," *German Microwave Conference Digest of Papers*, 227–230, Berlin, 2010.
2. Horii, Y., T. Hayashi, and Y. Iida, "A novel composite right/left-handed transmission line composed of cylindrical left-handed unit cells," *IEEE MTT-S International Microwave Symposium Digest*, 1013–1016, San Francisco, CA, 2006.
3. Engheta, N. and R. W. Ziolkowski, "A positive future for double-negative metamaterials," *IEEE Trans. Microw. Theory Tech.*, Vol. 53, No. 4, 1535–1556, 2005.
4. Ziolkowski, R. W., "Double negative metamaterial design, experiments, and applications," *IEEE Antennas and Propagation Society International Symposium*, Vol. 2, 396–399, 2002.
5. Duan, Z., B.-I. Wu, S. Xi, H. Chen, and M. Chen, "Research progress in reversed Cherenkov radiation in double-negative metamaterials," *Progress In Electromagnetics Research*, Vol. 90, 75–87, 2009.
6. Smith, D. R., W. J. Padilla, D. C. Vier, et al., "Composite medium with simultaneously negative permeability and permittivity," *Phys. Rev. Lett.*, Vol. 84, No. 18, 4184–4187, May 2000.
7. Decoopman, T., O. Vanbesien, and D. Lippens, "Demonstration of backward wave in a single split ring resonator and wire loaded finline," *IEEE Microw. Wireless Compon. Lett.*, Vol. 14, No. 11, 507–509, Nov. 2004.
8. Decoopman, T., A. Marteau, E. Lheurette, et al., "Left-handed electromagnetic properties of split-ring resonator and wire lzoaded transmission line in a fin-line technology," *IEEE Trans. Microw. Theory Tech.*, Vol. 54, No. 4, 1451–1457, Apr. 2006.
9. Salehi, H. and R. R. Mansour, "A new realization of left-handed transmission lines employing a coaxial waveguide structure," *IEEE MTT-S Int. Dig.*, 1941–1944, Long Beach, CA, Jun. 2005.
10. Saleh, H. and R. R. Mansour, "Analysis, modeling, and applications of coaxial waveguide-based left-handed transmission lines," *IEEE Trans. Microw. Theory Tech.*, Vol. 53, No. 11, 3489–3497, Nov. 2005.
11. Caloz, C., H. Okabe, T. Iwai, et al., "Transmission line approach of left-handed (LH) material," *Proc. USNC/URSI Nat. Rad. Sci. Meeting*, 39, San Antonio, TX, Jun. 2002.
12. Eleftheriades, G. V., A. K. Iyer, and P. C. Kremer, "Planar negative refractive index media using periodically L-C loaded transmission lines," *IEEE Trans. Microw. Theory Tech.*, Vol. 50, No. 12, 2701–2712, Dec. 2002.
13. Alibakhshi-Kenari, M., M. Naser-Moghadasi, R. A. Sadeghzadeh, et al., "Periodic array of complementary artificial magnetic conductor metamaterials-based multiband antennas for broadband wireless transceivers," *IET Microwaves, Antennas & Propagation*, Vol. 10, No. 15, 1682–1691, 2016.
14. Alibakhshikenari, M., B. S. Virdee, and E. Limiti, "Compact single-layer traveling-wave antenna designusing metamaterial transmission lines," *Radio Science*, Vol. 52, 1510–1521, 2017.
15. Sabah, C., "Composition of non-concentric triangular split ring resonators and wire strip for dual-band negative index metamaterials," *IEEE Microwave Symposium*, 303–306, 2010.
16. Xu, H. X., G. M. Wang, C. X. Zhang, et al., "Multi-band left-handed metamaterial inspired by tree-shaped fractal geometry," *Photonics & Nanostructures Fundamentals & Applications*, Vol. 11, No. 1, 15–28, 2013.
17. Fiori, M., P. Musé, and G. Sapiro, "Topology constraints in graphical models," *Advances in Neural Information Processing Systems*, 791–799, 2012.
18. Songsiri, J. and L. Vandenberghe, "Topology selection in graphical models of autoregressive processes," *Journal of Machine Learning Research*, Vol. 11, No. 2, 2671–2705, 2014.
19. Sajith, K., J. Gandhimohan, and T. Shanmuganantham, "Design of SRR loaded octagonal slot CPW fed wearable antenna for EEG monitoring applications," *Proceedings of IEEE International Conference on Circuits and Systems (ICCS)*, 49–53, Thiruvananthapuram, 2017.

20. Haghighi, S. S., A. Heidari, and M. Movahhedi, "A three-band substrate integrated waveguide leaky-wave antenna based on composite right/left-handed structure," *IEEE Transactions on Antennas and Propagation*, Vol. 63, No. 10, 4578–4582, Oct. 2015.
21. Alibakhshi-Kenari, M., M. Naser-Moghadasi, R. Ali Sadeghzadeh, et al., "Hexa-band planar antenna with asymmetric fork-shaped radiators for multiband and broadband communication applications," *IET Microwaves, Antennas & Propagation*, Vol. 10, No. 5, 471–478, 2016.
22. Alhawari, A. R. H., A. Ismail, and M. A. Mahdi, "Compact ultra-wideband metamaterial antenna," *Proceedings of 16th Asia-Pacific Conference on Communications (APCC)*, 64–68, Auckland, New Zealand, Oct. 31–Nov. 3, 2010.
23. Alibakhshi-Kenari, M., B. S. Virdee, P. Shukla, et al., "Interaction between closely packed array antenna elements using metasurface for applications such as MIMO systems and synthetic aperture radars," *Radio Science*, Vol. 53, No. 11, 1368–1381, 2018.
24. Alibakhshi-Kenari, M., B. S. Virdee, P. Shukla, et al., "Antenna mutual coupling suppression over wideband using embedded periphery slot for antenna arrays," *Electronics*, Vol. 7, No. 9, 198, 2018.
25. Alibakhshi-Kenari, M., B. S. Virdee, C. H. See, et al., "Study on isolation improvement between closely packed patch antenna arrays based on fractal metamaterial electromagnetic bandgap structures," *IET Microwaves, Antennas & Propagation*, Vol. 12, No. 14, 2241–2247, 2018.